Fast Simulation of Spin Transfer Torque Devices in a General Purpose TCAD Device Simulator

Frederik Ole Heinz
Synopsys Schweiz GmbH
Thurgauerstr. 40
CH-8050 Zürich
Switzerland
Email: fheinz@synopsys.com

Lee Smith
Synopsys Inc.
700 E. Middlefield Road
Mountain View, CA 94043
United States of America
Email: lees@synopsys.com

***Abstract*—We present integrated simulation of spin-transfer torque (STT) devices within the framework of a general purpose TCAD device simulator. A fast Airy function based approach is used to calculate spin and charge transport through magnetic tunnel junctions (MTJ). This enables direct mixed mode simulation of STT devices in a circuit environment — consisting of physical TCAD device models, SPICE-like compact models or a combination thereof — without first constructing a response surface model for the STT device. This was used to simulate a 4T-2MTJ non-volatile SRAM cell. For device interactions that are not captured in a circuit picture, STT and conventional devices may be combined in a single simulation geometry. Using an explicit exchange term in the Landau-Lifshitz-Gilbert equation allows capturing some aspects of spin dynamics beyond the macro-spin approximation.**

I. Introduction

As interest in spin-based devices and especially spin-transfer torque (STT) based memory is growing, it appears essential to provide simulation support for these novel devices not just through special purpose tools, but inside a general purpose TCAD device simulator. To this end, we have added simulation capabilities for STT devices to Sentaurus Device [1].

II. The Operating Principle of STT Devices

STT devices are based on the interaction of the spin of conduction electrons and the magnetization in ferromagnetic regions: electrons that are traveling through a ferromagnetic material are subject to (partial) polarization of the direction of their spin; this causes the tunneling current between two ferromagnetic regions separated by a thin insulator — a configuration know as a *magnetic tunnel junction* (MTJ), see Figure 1 — to become a function of the angle between the magnetization directions on either side of the barrier: parallel (P) alignment of the magnetization in both layers gives rise to a lower tunneling resistance than an anti-parallel (AP) magnetization configuration. Conversely, the flow of spin-polarized electrons is accompanied by the transport of angular momentum ("*spin current*"); angular momentum conservation during the absorption of spin current in a ferromagnetic region may change the magnetization direction ("*spin transfer torque*"). [2]

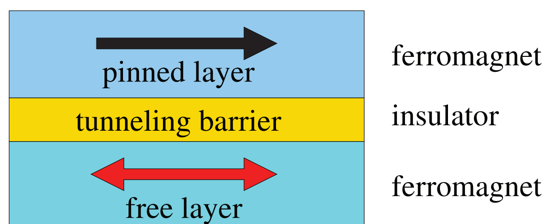

Fig. 1. Structure of a magnetic tunnel junction (MTJ): two ferromagnetic layers are separated by a thin insulating layer. The tunneling resistance of this structure will depend on the relative orientation of the magnetization in the two ferromagnetic layers.

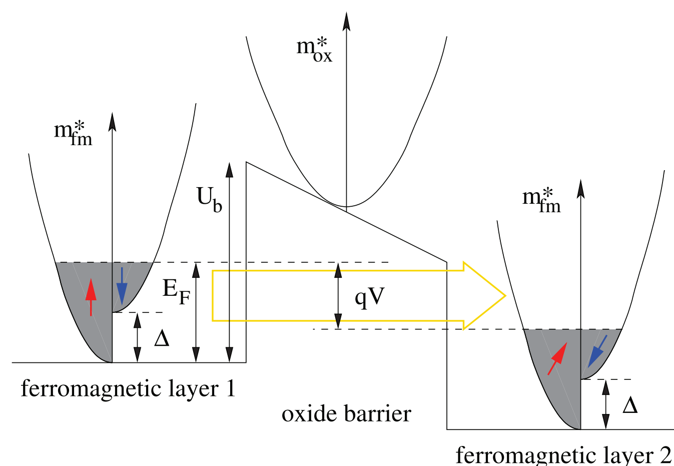

Fig. 2. Schematic band diagram of a MTJ. The tunneling model is characterized by effective electron masses m^* in the ferromagnet and the barrier, the position of the Fermi energy E_F relative to the band-edge, the barrier height U_b and the spin-splitting energy Δ.

III. Modeling of STT Devices

The modeling of STT devices requires coupled transient simulations of the magnetization dynamics inside ferromagnetic regions and of the spin-dependent tunneling transport of charge and angular momentum (electron spin) through thin layers of insulating material between ferromagnetic regions.

A. Spin-selective Tunneling

A spin-aware tunneling model is necessary to calculate the magnetization dependent currents and spin-injection rates for

978-1-4673-5736-4/13/$31.00 ©2013 IEEE

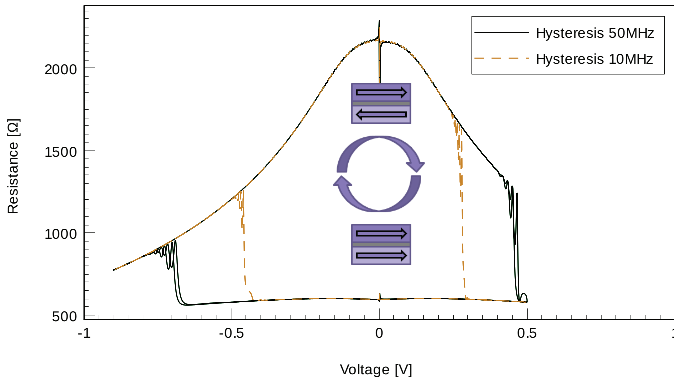

Fig. 3. Frequency dependence of resistance–voltage hysteresis curves of an i-MTJ (top layer: pinned magnetization; bottom layer: free magnetization). A negative offset is added to the the sinusoidal applied voltage to prevent the emergence of persistent oscillations during anti-parallel (AP) to parallel (P) switching of the magnetization (cf. Figure 5).

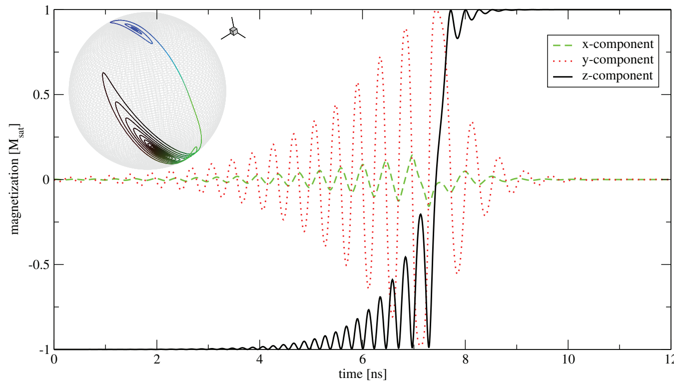

Fig. 4. Time dependence of the free layer magnetization of a MTJ at fixed applied voltage

a magnetic tunnel junction. The scalar wavefunctions of a non-magnetic system are replaced with two-component spinor wavefunctions to keep track of the spin state of the tunneling electrons. Inside the ferromagnetic region, "spin-up" and "spin-down" electrons are separated by an energy splitting Δ. The schematic band diagram assumed for modeling the tunneling through a MTJ is depicted in Figure 2. Each ferromagnetic layer defines its own "spin-up" and "spin-down" direction depending on the local direction of magnetization. Therefore, a "spin-up" electron on the left side of the barrier will in general correspond to a mixture of "spin-up" and "spin-down" states on the right side of the barrier, depending on the angle between the two magnetization directions..

B. Magnetization Dynamics

The magnetization dynamics of free magnetic layers is modeled by solving the Landau-Lifshitz-Gilbert (LLG) equation. Spin injected through the MTJ gives rise to an additional spin-transfer torque term [3]. In macro-spin approximation, the equation can be written as

$$\dot{\mathbf{M}} = -|\gamma|\mu_0 \mathbf{M} \times \mathbf{H}_{\text{eff}} + \frac{\alpha}{M_{\text{sat}}} \mathbf{M} \times \dot{\mathbf{M}} + \underbrace{\frac{|\gamma|\boldsymbol{\Gamma}}{V}}_{\text{STT}}, \quad (1)$$

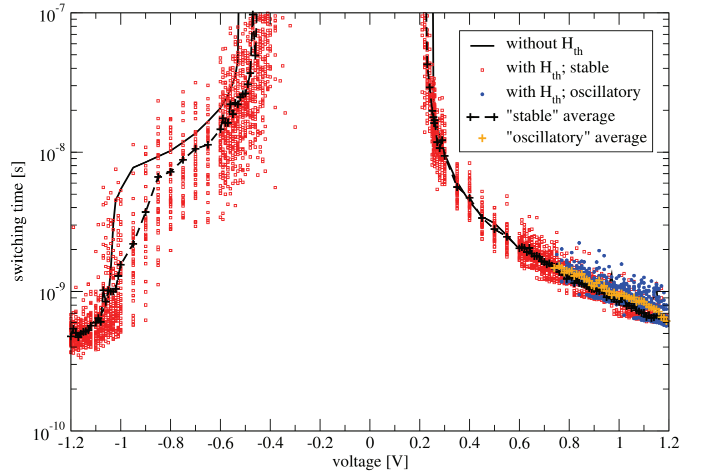

Fig. 5. Voltage dependence of the switching time of an i-MTJ (statistical run with 40 samples per voltage value); $V < 0$: P→AP switching; $V > 0$: AP→P switching.Under P→AP switching, the presence of the stochastic thermal fluctuation field $\mathbf{H}_{\text{th}}$ reduces the average switching time; for AP→P switching, switching times with thermal fluctuations symmetrically scatter around the fluctuation-free result. Above $\approx$0.7 V stationary precession may prevent the junction from settling down into a stable final state; in p-MTJs we did not observe this effect.

where $\mathbf{M}$ is the free layer magnetization, $|\mathbf{M}| = M_{\text{sat}}$ is the saturation magnetization of the material, γ is the gyromagnetic ratio that relates angular momentum to magnetic moment, and α is the phenomenological Gilbert damping coefficient. The effective magnetic field $\mathbf{H}_{\text{eff}}$ is proportional to the derivative of the magnetic energy $U(\mathbf{M})$ w.r.t. the magnetization; for STT-based memory devices, U is a strongly anisotropic function of the magnetization direction with two energetically favorable magnetization directions (e.g., along $\hat{\mathbf{e}}_z$ and $-\hat{\mathbf{e}}_z$)[1], separated by an energy barrier. Finally, $\boldsymbol{\Gamma}$ in the STT term is the rate at which angular momentum from tunneling electrons is absorbed by the free layer, and V is the free layer volume.

C. Hysteresis and Switching Threshold in MTJs

Together, the MTJ tunneling model and the LLG equation describe STT induced magnetization switching and tunneling magneto-resistance, the main constituents of STT-RAM operation. Figure 3 illustrates that the resistance of a MTJ exhibits hysteresis as a function of the applied voltage. The magnetization does not instantaneously follow the applied junction voltage (see Figure 4); this causes a frequency dependence in the hysteresis behavior. The effect of thermal fluctuations on the magnetization dynamics can optionally be included in the simulation by adding a stochastic noise term to $\mathbf{H}_{\text{eff}}$ in the LLG equation [4]. Figure 5 shows the switching delay of an in-plane MTJ[2] as function of the applied voltage both with and without thermal fluctuations.

IV. Performance Considerations

In order to speed up the calculation of spin-selective tunneling currents, an Airy function based expansion of the spinor-

[1] depending on the orientation of the favorable magnetization directions relative to direction of the this films, MTJs are classified as in-plane (i-MTJ) or perpendicular (p-MTJ).

[2] Perpendicular MTJs are much less susceptible to thermal effects.

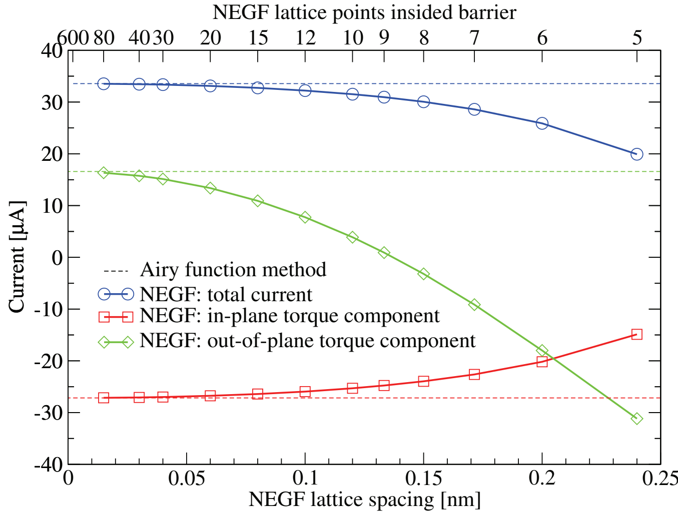

Fig. 6. Lattice convergence of NEGF results for MTJ tunneling current and its spin components to the Airy function based result; junction bias: 0.1 V.

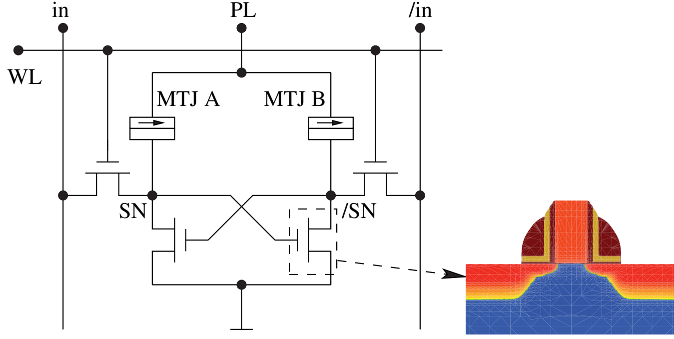

Fig. 7. Circuit diagram of a 4T-2MTJ nv-SRAM cell (cf. [7]). Transistors are modeled as 2D TCAD devices (mesh shown); MTJs are modeled as 1D devices.

wavefunctions of the MTJ was applied instead of the numerical NEGF method frequently used elsewhere (e.g., [5]). In combination with parallelization this reduces the wall-clock time for the evaluation of the tunneling integral (including integration over the wave number parallel to the interface) from minutes to a fraction of a second. The simulation time is further reduced by an automatic results caching and interpolation mechanism. The Airy based implementation was validated both by comparison to an in-house implementation of the NEGF method (see Figure 6) and literature results [5].

V. Mixed Mode Simulation of Hybrid Circuits

It is often important to study STT devices not in isolation but within their circuit environment. In contrast to pure circuit simulators enhanced to include the state variables of non-volatile (nv) memory devices, our approach allows all devices in the circuit to be described either by compact models or as full physical TCAD models. Also, simulation is fast enough for direct mixed simulations; construction of a parametrized MTJ response surface model as in [6] is not needed.

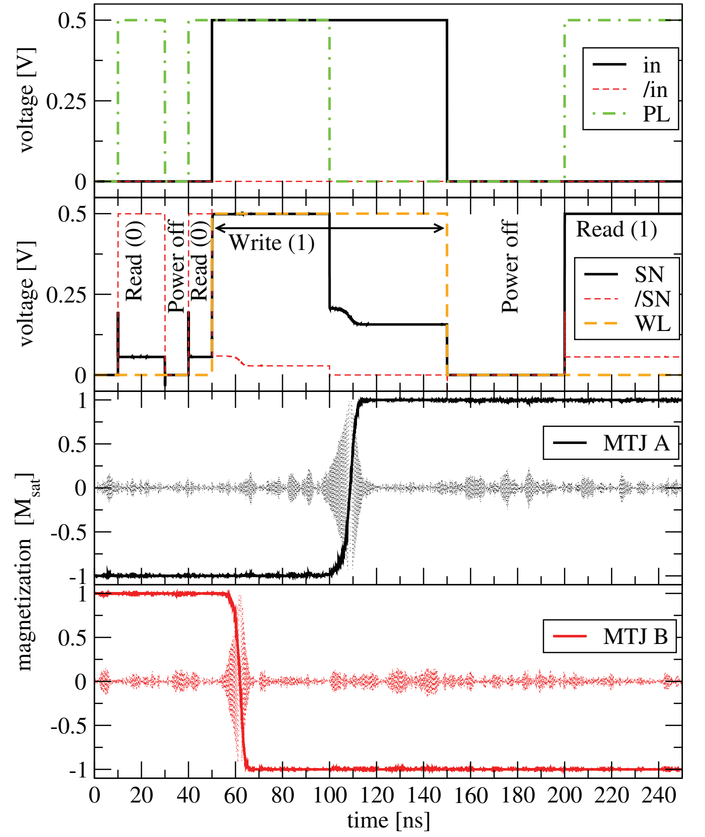

Fig. 8. Mixed-mode simulation of a 4T-2MTJ nv-SRAM cell similar to [7]; transistors and p-MTJs are modeled as physical TCAD devices, not SPICE-like compact models. Thermal fluctuations included by adding a Langevin term to $\mathbf{H}_{\text{eff}}$ in the LLG equation.

A. Simulation of a 4T-2MTJ nv-SRAM cell

As example circuit for demonstrating fully coupled mixed mode simulation with STT devices we use a non-volatile SRAM cell with four transistors and two MTJs similar to the one presented in [7]. The circuit layout of this cell is shown in Figure 7. At the center of the cell, there is a pair of cross-coupled transistors; each of these transistors is series-connected to a MTJ to form a voltage divider. The circuit nodes between MTJ and transistor are the *storage node* `SN` (below MTJ A) and the *complementary storage node* `/SN` (below MTJ B). This latching circuit is surrounded by a pair of selection transistors that are gated by the *wordline* `WL` and connect `SN` with the *bitline* `in` and `/SN` with the *complementary bitline* `/in`, respectively. Both MTJs and all four transistors are modeled as geometry based TCAD models. The following switching cycle is simulated (see Figure 8 for results):

1) Initially, power is off.
   MTJ A is in AP state, MTJ B in P state.
2) $t = 10$ns — Turn on power (`PL`→“1”).
   Since $R_{\text{MTJ A}} > R_{\text{MTJ B}}$, the left transistor of the latch becomes conductive and the right transistor blocks ⇒ `SN`⇝“0”, `/SN`⇝“1” (logical “0” detected).
3) $t = 30$ns — Power is turned off (`PL`→“0”).
4) $t = 40$ns — Power is restored (`PL`→“1”).
   The cell still in `SN`=“0” state (“Read (0)”).
5) $t = 50$ns — Store a logical “0”.
   Present data: `in`→“1”, `/in`→“0”, `WL`→“1”;

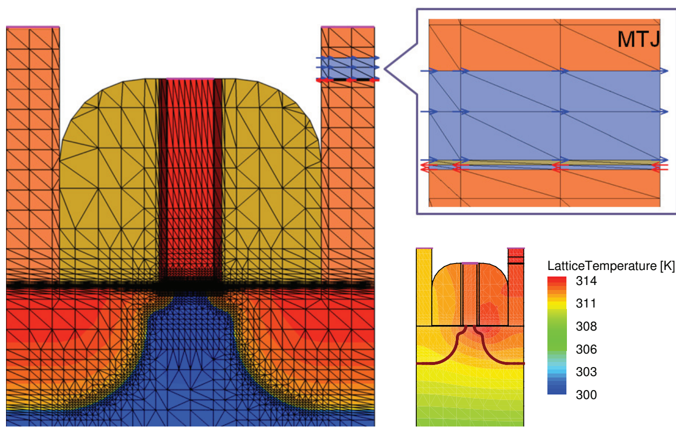

Fig. 9. A MOSFET and a MTJ combined on a single 2D device simulation geometry. Device structure and simulation results of a coupled simulation including self-heating.

the write operation has two sub-phases:

a) `PL`→"1". Electrons are injected from the free layer into the pinned layer of MTJ B
⇒ Parallel to anti-parallel switching.

b) `PL`→"0". Electrons are injected from the pinned layer into the free layer of MTJ A
⇒ Anti-parallel to parallel switching.

6) $t = 150$ns: Power off (`PL`→"0").

7) $t = 200$ns: Power is restored (`PL`→"1").
This time, $R_{\text{MTJ A}} < R_{\text{MTJ B}}$. The left latch transistor blocks and the right transistor becomes conductive ⇒ `SN`→"1", `/SN`→"0" (logical "1" detected).

VI. Integrated Simulation of Electronic and Spintronic Devices

Integrated simulation of conventional electronic devices and STT devices on the same simulation geometry (cf. Figure 9) allows the modeling of device interactions are not captured at the circuit model, for example thermal proximity effects.

VII. Magnetization Dynamics beyond the Macro-Spin Approximation

The above results were obtained using the *macro-spin approximation*: the exchange interaction is much stronger than all other magnetic effects; consequently, each ferromagnetic region is treated as a single, perfectly aligned magnetic domain; a single magnetization vector $\mathbf{M}$ completely describes the magnetization of the entire region. This is only exact for special geometries like an extended thin film stack or ellipsoidal ferromagnetic regions [8]. In general, the magnetization will be a vector field $\mathbf{M}(\mathbf{r})$ shaped by competition between the exchange interaction and the demagnetizing field. Even without considering the non-locality of the demagnetizing field, some micromagnetics effects like the generation of spin waves can be captured by including an exchange term $\mathbf{H}_{\text{ex}} = \frac{2A}{\mu_0 M_{\text{sat}}^2}\nabla^2\mathbf{M}$ in the effective field $\mathbf{H}_{\text{eff}}$ of the LLG equation. This allows modeling the non-local switching behavior of more complicated devices like the spin-torque majority gate [9] shown in Figure 10.

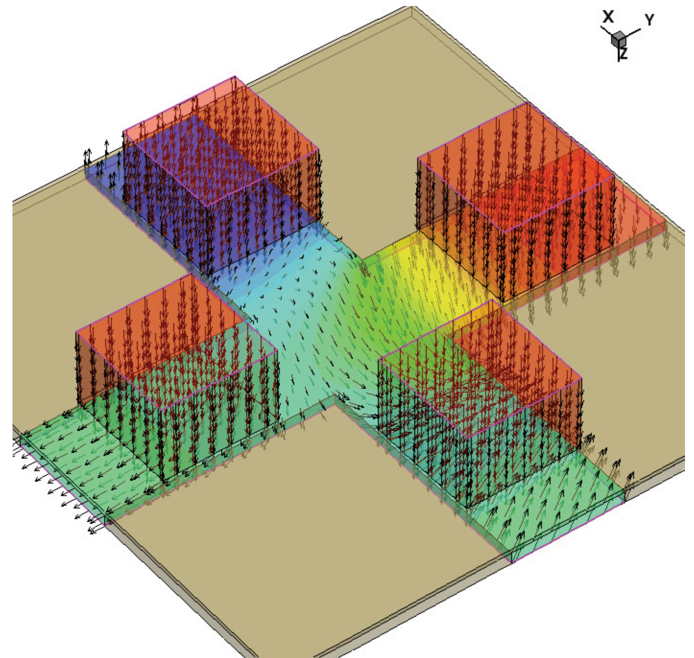

Fig. 10. Snapshot of the position dependent magnetization in a spin-torque majority gate similar to the device suggested in [9]. The pinned layer is split into four pieces; MTJs with different applied voltages compete for switching of the cross-shaped free layer. The bottom of the structure is grounded.

VIII. Conclusion

We implemented magnetization dynamics and spin-dependent tunneling using a fast Airy function approach. Via integration into a general purpose TCAD framework this enables simulation of individual STT cells and small hybrid circuits like an MTJ assisted nv-SRAM cell; coupling with advanced TCAD models for deep sub-micron devices, is possible. Device simulation engineers will be able to build upon accustomed procedures and work-flows and yet have access to STT effects.

References

[1] Sentaurus Device User Guide H-2013.03, Synopsys Inc., Mountain View, USA, 2013.

[2] D. C. Ralph and M. D. Stiles, "Spin transfer torques", Journal of Magnetism and Magnetic Materials, vol. 320, no. 7, pp. 1190–1216, 2008.

[3] J. C. Slonczewski, "Conductance and exchange coupling of two ferromagnets separated by a tunneling barrier", Phys. Rev. B, vol. 39, pp. 6995–7002, 1989.

[4] W. F. Brown, "Thermal Fluctuations of a Single-Domain Particle", Phys. Rev., vol. 130, pp. 1677–1686, 1963.

[5] Y. Hiramatsu, *et al.*, "NEGF Simulation of Spin-Transfer Torque in Magnetic Tunnel Junctions", IEEE International Meeting on the Future of Electron Devices, 2011.

[6] X. Fong, *et al.*, "KNACK: A Hybrid Spin-Charge Mixed Mode Simulator for Evaluating Different Genres of Spin-transfer Torque MRAM Bit-cells, SISPAD, 2011.

[7] T. Ohsawa, *et al.*, "1Mb 4T-2MTJ Nonvolatiole STT-RAM for Embedded memories Using 32b Fine-Grained Power Gating Technique with 1.0ns/200ps Wake-up/Power-off Times"; IEEE Symposion on VLSI Circuits, Digest of Technical Papers, 2012.

[8] J. A. Osborn, "Demagnetizing Factors of the General Ellipsoid", Phys. Rev., vol. 67, no. 11, pp. 351–357, 1945.

[9] D. E. Nikonov, G. I. Bourianoff, T. Ghani, "Proposal of a Spin-Torque Majority Gate Logic", EDL, vol. 32, pp. 1128-1130, 2011.